JACS
JOURNAL OF THE AMERICAN CHEMICAL SOCIETY

pubs.acs.org/JACS

Article

Triplex-Forming Peptide Nucleic Acid Controls Dynamic Conformations of RNA Bulges

Christopher A. Ryan, Md Motiar Rahman, Vipin Kumar, and Eriks Rozners*

Cite This: J. Am. Chem. Soc. 2023, 145, 10497−10504

Read Online

ACCESS | Metrics & More | Article Recommendations | Supporting Information

ABSTRACT: RNA folding is driven by the formation of double-helical segments interspaced by loops of unpaired nucleotides. Among the latter, bulges formed by one or several unpaired nucleotides are one of the most common structural motifs that play an important role in stabilizing RNA−RNA, RNA−protein, and RNA−small molecule interactions. Single-nucleotide bulges can fold in alternative structures where the unpaired nucleobase is either looped-out (flexible) in a solvent or stacked-in (intercalated) between the base pairs. In the present study, we discovered that triplex-forming peptide nucleic acids (PNAs) had unusually high affinity for single-purine-nucleotide bulges in double-helical RNA. Depending on the PNA's sequence, the triplex formation shifted the equilibrium between looped-out and stacked-in conformations. The ability to control the dynamic equilibria of RNA's structure will be an important tool for studying structure−function relationships in RNA biology and may have potential in novel therapeutic approaches targeting disease-related RNAs.

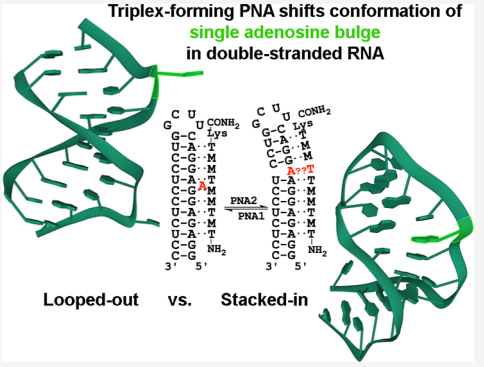

INTRODUCTION

RNA forms highly complex secondary and tertiary structures that rival the intricacy of proteins. Structured RNAs play important roles in the biology of healthy cells and development of disease. RNA has been a central component in recent novel discoveries of exciting biology, such as CRISPR,[1,2] as well as new diseases impacting the global community, such as SARS-CoV-2.[3,4] Chemical tools that could sequence specifically recognize folded RNAs to modulate their structure and function will find broad applications in medicine and biotechnology. However, such tools are not generally available because recognition of folded structurally complex RNA molecules remains a formidable problem either for small molecules[5,6] or for oligonucleotide ligands.[7,8] Recently, we[9−11] and other research groups[12−16] explored the use of triplex-forming peptide nucleic acid (PNA, Figure 1) for sequence-specific recognition of double-stranded RNA (dsRNA).[17,18] Herein, we report a surprising discovery that PNA forms unusually stable complexes with dsRNA having purine nucleotide bulges.

RNA bulges are one of the most common features of complex dsRNA folds.[19] The simplest and most common bulge is formed when one strand of dsRNA has an additional nucleotide that lacks a base pairing partner on the other strand. More complex bulges formed by several unpaired nucleotides are also abundant and play important roles in intermolecular recognition of RNA by proteins and other RNA molecules.[19] The unpaired nucleotides forming the bulge may adopt either looped-out or stacked-in conformations. The former is flexible and may adopt various structures being either extruded in the solvent or folding back in the major or minor groves of dsRNA. In the latter, stacked-in bulge nucleotides are usually engaged in non-canonical hydrogen bonding (e.g., base triplets) with the Watson−Crick base pairs present in the stem. Both conformations may be present in a dynamic equilibrium that depends on a subtle balance of stabilizing and destabilizing forces, most importantly, a strong preference of dsRNA to maintain continuous stacking interactions throughout the bulge motif. Herein, we report an intriguing observation that triple-helical binding of PNA can shift the equilibrium between looped-out and stacked-in conformations depending on the sequence of PNA.

PNAs are synthetic DNA analogues developed in the 1990s as triplex-forming ligands for recognition of dsDNA.[20] Surprisingly, instead of forming the expected PNA−dsDNA triplex, PNA invaded dsDNA clamping on to the purine-rich strand, forming a PNA/DNA/PNA complex, and displacing the pyrimidine-rich strand as an unpaired loop.[21] While the majority of DNA recognition studies followed up on this exciting discovery, the original intent of forming PNA−dsDNA triplexes is also actively explored.[18] Except for an early report on a weak complex of PNA with an HIV-1 RNA hairpin,[22]

Received: November 23, 2022
Published: May 8, 2023

https://doi.org/10.1021/jacs.2c12488
J. Am. Chem. Soc. 2023, 145, 10497−10504

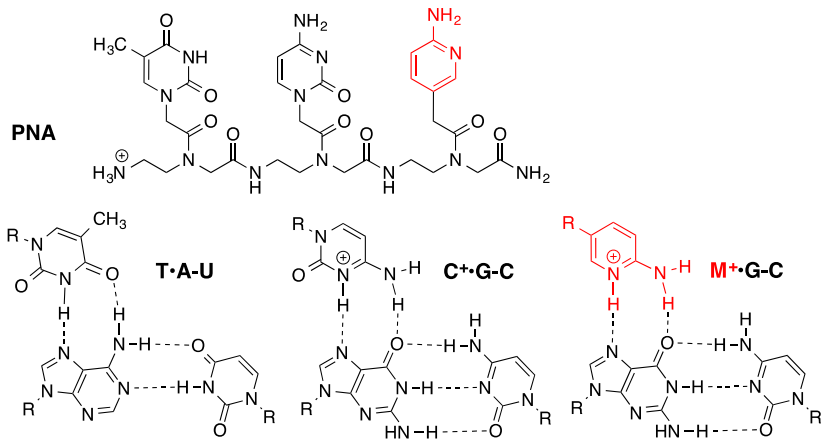

Figure 1. Structures of PNA and Hoogsteen triplets.

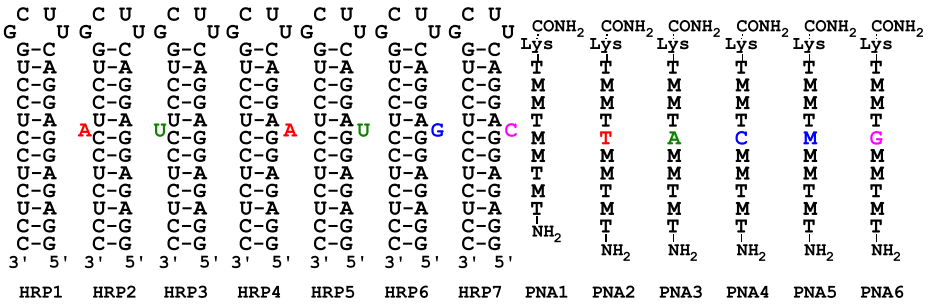

Figure 2. Sequences of dsRNA hairpins having single-nucleotide bulges and PNA ligands: PNA1 matching HRP1 and PNA2−PNA6 having one additional nucleobase targeting the bulged nucleotide in HPR4−HRP7. Potential matched pairing (Watson−Crick or Hoogsteen) between the bulging nucleotide and extended PNA base is indicated by matched color.

Table 1. Affinity of Triplex-Forming PNAs for dsRNA Hairpins Featuring Single-Nucleotide Bulges (Figure 2) Measured Using ITC

PNA[a] (extra base)	HRP1 (no bulge)	HRP2 (A)	HRP3 (U)	HRP4 (A)	HRP5 (U)	HRP6 (G)	HRP7 (C)
PNA1 (none)	**30 ± 2**	55 ± 2	42 ± 2	52 ± 1	38 ± 2	39 ± 2	33 ± 1
PNA2 (T)	4.6 ± 0.1	3.6 ± 0.2	7.1 ± 0.7	**220 ± 7**	14 ± 1	37 ± 1	16 ± 1
PNA3 (A)	1.6 ± 0.1	ND[b]	ND[b]	35 ± 1	23 ± 1	35 ± 1	25 ± 1
PNA4 (C)	3.1 ± 0.1	ND[b]	ND[b]	14 ± 1	5.7 ± 0.3	**97 ± 5**	7.1 ± 0.4
PNA5 (M)	11 ± 1	ND[b]	ND[b]	34 ± 2	19 ± 1	**104 ± 1**	12 ± 1
PNA6 (G)	4.3 ± 0.3	ND[b]	ND[b]	27 ± 1	21 ± 1	27 ± 1	24 ± 1

[a]Association constants, $K_a \times 10^6$ M^{-1}, average of three experiments ± stand. dev., for binding of PNAs to the respective hairpins in 50 mM potassium phosphate buffer (pH 7.4) containing 2 mM $MgCl_2$, 90 mM KCl, and 10 mM NaCl at 25 °C. [b]ND—no data, not measured.

binding of PNA to dsRNA had not been studied until 2010 when our group discovered that PNA formed unusually stable and sequence-specific triple helices with dsRNA.[23] Follow-up studies from our group and others reported improvements in binding affinity under physiological salt and pH conditions[9−11,13] and improved sequence scope using nucleobase modifications.[16,24] Most notably, using 2-aminopyridine (M base, $pK_a \sim 6.7$) instead of cytosine ($pK_a \sim 4.5$) removed the requirement for slightly acidic conditions to form C+•G−C Hoogsteen triplets (Figure 1), enabling the formation of stable PNA−dsRNA triple helices having M+•G−C triplets at physiological pH and salt concentration.[9−11] In these earlier experiments, we noticed that M-modified PNAs were binding strongly not only to perfectly Watson−Crick hydrogen-bonded dsRNA but also to RNA helices containing non-canonical base pairs and even bulges.[9,25] These observations inspired the present systematic study of triple-helical recognition of single-nucleotide bulges in dsRNA.

Herein, we report that PNAs formed unusually stable and sequence-specific triple helices with single-purine-nucleotide bulges in model dsRNA hairpin systems. Chemical probing of the RNA structure confirmed that the triplex formation shifted the equilibrium between looped-out and stacked-in conformations depending on the PNA's sequence. The ability to control the dynamic equilibria of the structured RNA will be an important tool for basic RNA biology and may have potential in therapeutic targeting of RNAs.

https://doi.org/10.1021/jacs.2c12488
J. Am. Chem. Soc. 2023, 145, 10497−10504

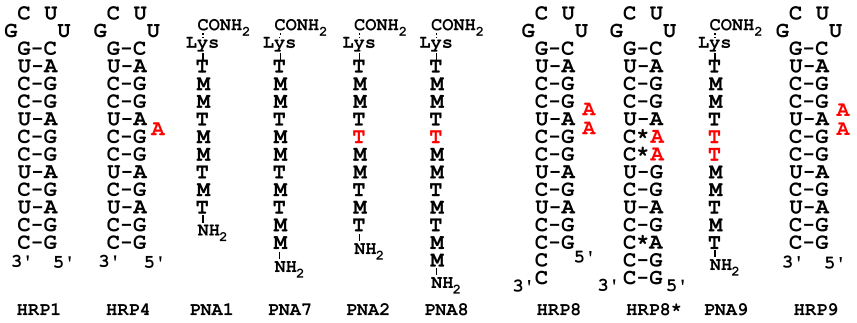

Figure 3. Sequences of dsRNA hairpins having one (left) or two (right) adenosine bulges and complimentary PNA ligands.

RESULTS AND DISCUSSION

Our study started with testing a hypothesis that triplex-forming PNAs would recognize a continuous helix of dsRNA despite the presence of a bulge formed by a single unpaired nucleoside. Our hypothesis assumed that the single nucleotide would adopt a looped-out conformation that would not significantly perturb the helical structure of RNA and hence would not interfere with triplex formation. To test this hypothesis, we modified the hairpin model system (HRP1, Figure 2) used in our previous studies[9−11] by adding one unpaired nucleotide (highlighted in color in Figure 2) either in the non-target pyrimidine strand (HRP2 and HRP3) or in the triplex-target purine strand (HRP4-HRP7). The stability of triple helices formed by PNAs with dsRNA hairpins in Figure 2 was measured using isothermal titration calorimetry (ITC) and UV thermal melting at 300 nm in a physiologically relevant buffer (pH 7.4) as previously reported.[9−11] Consistent with our earlier studies,[9−11] PNA1 formed a strong triplex (Table 1, K_a = 30 × 10^6 M^{-1}) with the perfectly matched HRP1.

Confirming our hypothesis, PNA1 formed equally strong triplexes with dsRNAs having single-nucleotide bulges (Table 1, first row). The ITC results in Table 1 were fully consistent with the UV thermal melting measurements on the same triplexes summarized in Table S14. These results supported our hypothesis that in triplexes formed by PNA1, the single nucleotide was looped-out of the continuous helical stack and did not interfere with the triple-helical recognition of the dsRNA target.

To test if the bulged nucleotide could be engaged in molecular recognition by the triplex-forming PNA, we inserted an additional T nucleobase in the PNA1 sequence giving PNA2 (red in Figure 2). As expected, this strongly lowered the affinity of PNA2 for HRP1−HRP3 as the extension of the PNA sequence created several mismatched triplets. To our surprise, PNA2 formed an unusually stable complex (red in Table 1, K_a = 220 × 10^6 M^{-1}) with HRP4 having a bulged A in the target strand. The 1:1 PNA/RNA stoichiometry observed in ITC experiments (n = 1, Table S3) was confirmed with a Job plot (Figure S29) and was consistent with the expected PNA1−HRP4 triple helix formation. The interaction was sequence specific as PNA2 had at least 6 times lower affinity for other hairpins, with PNA2−HRP6 being the second most stable, which may be explained by enhanced stacking and better H-bonding capability of bulged G (compared to U or C in HRP5 and HRP7, respectively).

These results suggested that the bulge adenosine in HRP4 was intercalated in the purine strand and involved in stabilizing interaction with the additional thymine in PNA2. Similar albeit slightly weaker interactions between the bulge G in dsRNA and C or M in PNA stabilized the PNA4−HRP6 and PNA5−HRP6 triplexes (blue in Table 1, K_a = 97 and 104 × 10^6 M^{-1}, respectively).

The strong stabilization of triple helices involving bulged nucleotides was fascinating, but the nature of interactions was not immediately obvious. Straightforward Watson−Crick pairing to the bulge nucleotides can be excluded because the reverse interaction of A with U or G with C did not result in unusually stable PNA3−HRP5 or PNA6−HRP7 triplexes (green and pink in Table 1). It is conceivable that T and C or M in PNAs engage the stacked-in unpaired A and G in Hoogsteen hydrogen bonding, as in T•A−U and M$^+$•G−C triplets; however, this cannot be the only interaction stabilizing the triplexes as we would expect M$^+$•G to be more stabilizing than T•A based on the relative stability of M$^+$•G−C and T•A−U triplets observed in our previous studies.[11] Moreover, compared to HRP1, PNA2−PNA6 consistently showed higher affinity for HRP2−HRP7 (Table 1), suggesting that the bulge nucleotide caused some structural change in the major groove that was favorable for binding of all PNAs.

The similar stability of PNA4−HRP6 and PNA5−HRP6 triplexes was initially unexpected because Hoogsteen hydrogen bonding requires protonation of both C and M. Under physiological pH, protonation would be favored only for M, which would result in PNA5−HRP6 triplex being more stable than the PNA4−HRP6 triplex as the latter has C interacting with bulge G. However, control experiments showed that substitution of one M$^+$•G−C with C$^+$•G−C triplet in either PNA1−HRP1 or PNA5−HRP6 complexes resulted in relatively small decreases in triplex stability (Figure S33, PNA1C and PNA5C, respectively), which was similar to the difference in the stability of PNA4−HRP6 and PNA5−HRP6 triplexes (Tables 1 and S14) and consistent with the hypothesized Hoogsteen pairing.

To get more insight into the binding of triplex-forming PNAs to RNA having a single-adenosine bulge, we compared the affinity of PNA1 and PNA2 with the affinity of PNA7 and PNA8 having two additional M nucleobases (Figure 3). Extension of the PNA−dsRNA triplexes with two additional M$^+$•G−C triplets gave a modest increase in binding affinity (c.f., PNA1 to PNA7 and PNA2 to PNA8 in Table 2). The effect ranged from a slight improvement for HRP1 to almost doubling the affinity toward HRP4. The ITC results were consistent with UV thermal melting (Table S15) that showed even less significant increase in PNA7 and PNA8 affinity, resulting from the two additional M bases.

The modest improvement by two additional M$^+$•G−C triplets was in a stark contrast to the unusually strong binding to a single adenosine bulge (c.f., PNA1−HRP1 to PNA2−

https://doi.org/10.1021/jacs.2c12488
J. Am. Chem. Soc. 2023, 145, 10497−10504

Table 2. Affinity of Triplex-Forming PNAs for dsRNA Hairpins in Figure 3

PNA[a] (extra base)	HRP1 (no bulge)	HRP4 (A)	HRP8 (AA)	HRP9 (AA)
PNA1 (none)	**30 ± 2**	52 ± 1	28 ± 1	27 ± 1[b]
PNA7 (none)	**43 ± 1**	101 ± 4	30 ± 1	ND[c]
PNA2 (T)	4.6 ± 0.1	**220 ± 7**	44 ± 2	42 ± 1[b]
PNA8 (T)	7.3 ± 0.1	**340 ± 10**	70 ± 3	ND[c]
PNA9 (TT)	1.7 ± 0.1	14 ± 1	**110 ± 3**	**108 ± 3**

[a]Association constants, $K_a \times 10^6$ M^{-1}, average of three experiments ± stand. dev., for binding of PNAs to the respective hairpins in 50 mM potassium phosphate buffer (pH 7.4) containing 2 mM $MgCl_2$, 90 mM KCl, and 10 mM NaCl at 25 °C. [b]Average of two replicates. [c]ND—no data, not measured.

HRP4 and PNA7−HRP1 to PNA8−HRP4) which resulted in an almost an order of magnitude increase in K_a (Table 2) and >10 °C increase in T_m (Table S15). Our previous study found that an M^+•G−C triplet was about 3 times stronger than a T•A−U triplet.[11] In the light of these results, it is remarkable that recognition of a single-adenosine bulge brings about a significantly larger increase in affinity than the addition of two M^+•G−C triplets.

To obtain insights into changes in the looped-out vs stacked-in conformation (Figure 4) upon PNA binding, we performed chemical probing of the secondary structure of HRP4 as part of a larger model RNA fragment (1Ab1 RNA, for details, see Figure S34). Dimethyl sulfate[26] (DMS, Figure 4B) and selective 2′-hydroxyl acylation analyzed by primer extension[27] (SHAPE) (Figure 4C) probing of HRP4 model RNA alone (no added PNA) showed no reactivity of A8 and significant reactivity of A9 and the adjacent G10. Consistent with our hypothesis, when probing was done in the presence of PNA1, the reactivity of A9 increased in both DMS and SHAPE experiments (Figure 4B,C, second lanes). These results suggested that in the absence of PNA, the bulge in HRP4 was in a dynamic equilibrium where A8 was stacked-in and A9 was partially looped-out. As we expected, binding of PNA1 shifted the equilibrium to a conformation having A9 (but not A8) looped-out.

Somewhat unexpectedly, binding of PNA2 to the HRP4 model resulted in little change in the reactivity of A9. It should be noted that all bands in the PNA2 lane were somewhat weaker than in other lanes because of the suppressed reverse transcriptase activity most likely by the residual PNA2 remaining bound to RNA during reverse transcription (for details, see Figure S34). A native gel shift (6% PAGE) assay showed one slightly shifted 1Ab1 RNA band appearing with increasing concentrations of PNA2 (Figure S36). At the concentrations used in chemical probing (5 μM 1Ab1 RNA and 15 μM PNA2), we did not observe any additional shifted bands indicating unusual structures. Normalized ImageJ quantification of bands in the chemical probing gels (numbers in Figure 4B,C, for details, see the legend of Figure S34) showed that the reactivity in the PNA2 lane was similar to that in the No PNA lane and the weakly binding ($K_a \sim 3 \times 10^6$ M^{-1}) scrambled PNA (PNAscr) lane. It is conceivable that a stacked-in A could still have its Watson−Crick face and 2′-hydroxyl available for DMS and SHAPE reactions, respectively, which may explain the unexpected remaining reactivity in the PNA2 lane.

Finally, we asked the question if triplex-forming PNAs can control the conformation of larger RNA bulges, such as the two-adenosine bulge in HRP8 (Figure 3). HRP8 having a two cytosine 3′-overhang was designed to have two alternative secondary structures, HRP8 having two adenosines looped-out or HRP8* where the 5′-strand shifts two nucleosides down to form a continuous helix with three non-canonical C*A base pairs and a U−G wobble pair. Binding of PNA1 and PNA7 to HRP8 (Table 2) was consistent with recognition of other dsRNAs having a single-nucleotide bulge and suggested that in these complexes, the two bulge adenosines were looped-out of the triplex. Binding of PNA2 and PNA8 resulted in a slight increase of binding affinity. Binding of PNA9 having two additional T nucleobases to HRP9 further increased the affinity. While the absolute stability of the PNA9−HRP8 triplex was lower than that of PNA2-HRP4 (Table 2, K_a = 110 vs 220 × 10^6 M^{-1}), the relative increase in affinity from bulge recognition was similar (~4-fold) when comparing PNA1−HRP4 vs PNA2−HRP4 and PNA1−HRP8 vs PNA9−HRP8.

Chemical probing of HRP8 as part of a larger model RNA fragment (2Ab5 RNA, Figure 5, for details, see Figure S35) showed that triplex-forming PNAs had more complex interactions with the two-adenosine bulge than was observed for a single-adenosine bulge in HRP4. In all complexes, A8 was unreactive and engaged in an A−U base pair. It should be

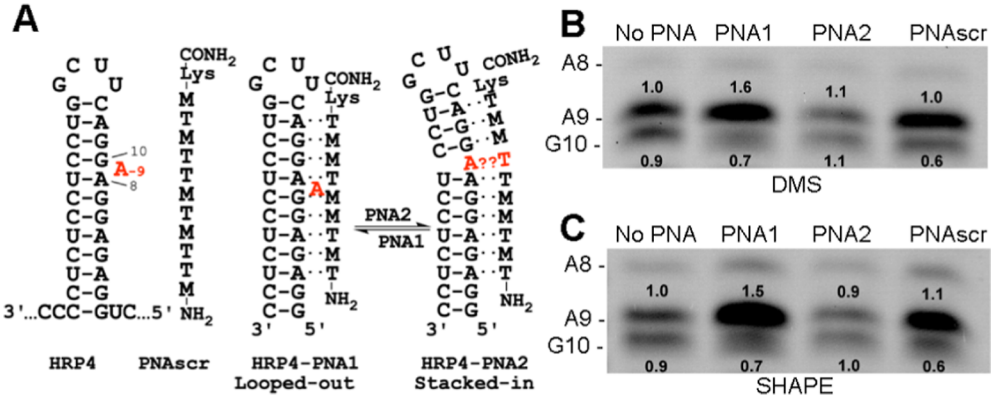

Figure 4. Chemical probing results of binding of triplex-forming PNAs to HRP4 embedded in a larger RNA sequence (1Ab1 RNA, for details, see Figure S34): (A) sequences of RNA and PNAs; (B) DMS probing of A8 through G10; and (C) SHAPE probing of A8 through G10. Numbers on gel images are normalized band intensities as quantified by ImageJ (for details, see the Supporting Information, page S47).

https://doi.org/10.1021/jacs.2c12488
J. Am. Chem. Soc. 2023, 145, 10497−10504

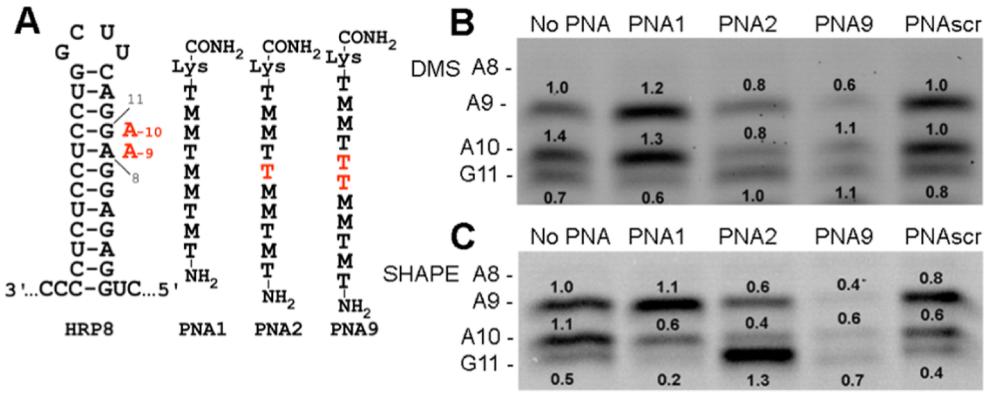

Figure 5. Chemical probing results of binding of triplex-forming PNAs to HRP8 embedded in a larger RNA sequence (2Ab5 RNA, for details, see Figure S35): (A) sequences of RNA and PNAs; (B) DMS probing of A8 through G11; and (C) SHAPE probing of A8 through G11. Numbers on gel images are normalized band intensities as quantified by ImageJ (for details, see the Supporting Information, page S47).

noted that overall, the bands in the PNA9 lane were significantly weaker than in other lanes because of suppressed reverse transcriptase activity most likely caused by the residual PNA9 remaining bound to RNA during reverse transcription (for details, see Figure S35). Normalized ImageJ quantification of the bands are given as numbers in Figure 5B,C (for details, see the legend of Figure S35).

In the absence of a PNA ligand, A9 and A10 showed significant reactivity consistent with a dynamic structure having both A9 and A10 at least partially looped-out. Binding of PNA1 slightly increased the DMS (Figure 5B) and SHAPE (Figure 5C) reactivity of A9 while decreasing the reactivity of A10. Interestingly, binding of PNA2 having only one additional T nucleobase and medium affinity ($K_a = 44 \times 10^6$ M^{-1}, Table 2) gave an unexpected probing pattern with decreased reactivity of both bulge adenosines but increased SHAPE reactivity of G11. Binding of PNA9 having two additional T nucleobases resulted in the expected lowered reactivity of both bulge adenosines. As for binding of PNA2 to 1Ab1 RNA, binding of PNA9 to 2Ab5 RNA resulted in only one slightly shifted band in the native gel shift (6% PAGE) assay (Figure S37). At the concentrations used in chemical probing (5 μM 2Ab5 RNA and 15 μM PNA9), we did not observe any additional shifted bands indicating unusual structures.

Finally, the scrambled PNA (PNAscr) decreased the reactivity of both bulge adenosines, suggesting that even a weakly binding ($K_a \sim 3 \times 10^6$ M^{-1}) PNA could decrease the conformational flexibility of RNA bulges. Neither DMS nor SHAPE showed any evidence for shifting of the helical register and forming the alternative PNA8−HRP8* triplex (no change in the reactivity of C31 in Figure S35). This result was further confirmed by a similar affinity of PNA8 for HRP8 and HRP9 that lacked the two-cytosine overhang and was not expected to favor shifting of the helical register. Overall, these results were consistent with the expected control of bulge conformation by the triplex-forming PNAs suggested by ITC and UV melting experiments. Chemical probing also indicated the formation of more complex structures for the two-adenosine bulge in HRP8 (e.g., unexpected reactivity of G11 in PNA2−HRP8) compared to the simpler single-adenosine bulge in HRP4.

To obtain more insights into structural features of bulge recognition by our PNAs, we recorded the CD spectra of the unusually stable complexes (Figure S38). Changes in CD signals upon binding of PNA1 and PNA2 to HRP4 were similar (Figure S38A) and consistent with our previously recorded CD spectra of PNA−dsRNA triplexes.[23] Overall, the CD signals for the PNA complexes with bulge-containing RNAs were similar and did not reveal any unusual features or large-scale structural changes (Figure S38B).

Collectively, our biophysical results are consistent with sequence-specific triple helical binding of PNAs to double-helical RNA having purine nucleotide bulges. The alternative binding mode, PNA invasion, and formation of the PNA−RNA−PNA triplex is unlikely given the 1:1 stoichiometry of complexes. Moreover, our recent study showed that M was not able to form stable M−G Watson−Crick base pair that would be required to support PNA−RNA invasion complexes.[11] Additional control experiments confirmed these expectations. Native gel shift (10% PAGE) assays showed only the expected shifts for PNA2−HRP4 (Figure S39) and PNA9−HRP9 triplexes (Figure S40). The assays showed no additional shifts due to strand invasion at higher PNA concentrations. ITC and UV melting experiments of PNA2 and PNA9 biding to single-stranded RNAs having the same sequence as the purine-rich strands of HRP1, HRP4, and HRP8 showed only weak interactions (Figures S41−S44) most likely caused by complex secondary structures of the purine-rich ssRNAs (suggested by UV melting of ssRNAs only at 295 nm in Figure S45). We did not observe ITC or UV signals that can be interpreted as the formation of PNA−ssRNA duplexes. While our current working hypothesis is that PNAs recognize bulged nucleotides through the Hoogtseen hydrogen-bonded triple helix, complete understanding of the unusually high stability of these complexes will require detailed structural studies.

CONCLUSIONS

Taken together, our results demonstrate the unique ability of triplex-forming PNAs to control the dynamic conformation of RNA's secondary structure. In contrast to DNA, RNA helices are not uniform but instead contain a variety of non-helical motifs, such as bulges, loops, and junctions that allow RNA to fold in complex tertiary structures. Among these, bulges formed by one or several unpaired nucleotides play an important role in stabilizing RNA−RNA, RNA−protein, and RNA−small molecule interactions.[19] For example, looped-out nucleotides are involved in long-range interactions stabilizing the RNA tertiary structure for interactions with proteins and co-factors.[19] Therefore, the ability to switch bulge conformation from stacked-in to looped-out and vice versa will be a highly useful tool for fundamental studies on RNA biology.

https://doi.org/10.1021/jacs.2c12488
J. Am. Chem. Soc. 2023, 145, 10497−10504

Recognition of RNA bulges is also expected to have significant therapeutic potential and has been explored using small molecules.[5,6] Small molecules bind RNA bulges using a subtle interplay of hydrogen bonding and stacking interactions that contribute to selectivity based on the sequence and shape of its binding site.[28] Despite significant success in using small molecules to recognize some therapeutically relevant RNAs, achieving high affinity and specificity for any sequence of complex RNA is still a formidable problem.[5,6,29−31] In the present study, we demonstrate an alternative approach to bulge recognition using triplex-forming PNAs as the major driver of affinity and specificity. Most remarkably, binding to a single-purine-nucleotide bulge resulted in surprisingly stable complexes. Our results also suggest that the shape of RNA at the bulge site may play an important but not a well-understood role in governing the affinity of PNA recognition of RNA bulges. For example, the triplex formation with a single A bulge resulted in a more stable complex than the triplex formation with a single G bulge, which is contrary to the established stabilities of Hoogsteen triplets.[9−11] Similarly, recognizing a single A bulge produced a greater stabilizing effect than recognizing both adenosines in a two A bulge. Most importantly, binding of triplex-forming PNAs switched the conformation of purine bulges in dsRNA between stacked-in and looped-out depending on the sequence of PNA. Our results suggest that triplex-forming PNAs may be unique tools to study structure−function relationships in RNA biology and have potential for designing new approaches to therapeutic RNA targeting.

EXPERIMENTAL SECTION

PNA Synthesis. The PNAs were synthesized on an Expedite 8909 synthesizer at a 2 μmol scale on a NovaSyn TG Sieber resin (Novabiochem) using methods previously developed in our group.[32] Commercial PNA monomers (A, G, T, and C) were purchased from Link Technologies. M monomer was synthesized using procedures previously described by our group.[9−11] PNAs were cleaved from the solid support using 0.6 mL of 20% m-cresol in TFA for 2 h using the two-syringe pull−push method. Crude PNA was separated in three Eppendorf tubes (200 μL in each); the resin was washed once more with 0.2 mL of 20% m-cresol in TFA. PNA was precipitated by the addition of chilled diethyl ether (∼1.0 mL) and incubation at −20 °C for 15 min, followed by centrifugation (15,000 rpm, 30 min). Ethyl ether was then removed using a pipette, and the PNA was washed once more with 1.0 mL of ethyl ether and centrifuged (15,000 rpm, 10 min). The ethyl ether was again decanted and the crude PNA, a white solid, was dissolved in 1.25 mL of 0.1% formic acid in water. Samples were then analyzed by LC/MS on a Shimadzu LC/MS-2020 system to confirm the synthesis, purified by HPLC on either a Shimadzu LC-20 or a LC-40 system, and finally reanalyzed by LC/MS to confirm their purity (Figures S1−S14, Table S1). Yields were quantified by absorbance at 260 nm using extinction coefficients of 15,400 M^{-1} cm^{-1} for A, 11,500 M^{-1} cm^{-1} for G, 8560 M^{-1} cm^{-1} for T, 7400 M^{-1} cm^{-1} for C, and 806 M^{-1} cm^{-1} for M. After PNA quantification, solutions were lyophilized and redissolved in nuclease-free water to a final concentration of 240 μM.

Stability of PNA−dsRNA Triplexes. Isothermal titration calorimetry experiments were done in triplicate on a MicroCal ITC200 instrument at 25 °C in 50 mM potassium phosphate buffer (pH 7.4) containing 2 mM $MgCl_2$, 90 mM KCl, and 10 mM NaCl. In a typical experiment 2.45 μL aliquots of PNA solution were sequentially injected from a 40 μL rotating syringe (750 rpm) into 200 μL of RNA hairpin solution. The standard concentration of PNA was 75 μM, and the standard concentration of RNA was 10 μM. For exceptionally tight binders, an additional replicate was performed at a lower concentration. The concentrations are indicated on relevant tables and figures in the Supporting Information. Results were analyzed using MicroCal PEAQ-ITC software to obtain quantitative thermodynamic binding data. Detailed results of individual experiments are given in Tables S2−S13 and Figures S15−S28 and are summarized in Tables 1 and 2.

UV thermal melting experiments were done on a Shimadzu UV-1800 or a UV-2600 spectrophotometer equipped with TMSPC-8 temperature controllers. A temperature ramp rate of 1.0 °C was used in all cases. Absorbance was monitored at 300 nm for triplex formation involving PNAs (18 μM). Experiments were performed in ITC buffer containing 50 mM potassium phosphate, 2 mM $MgCl_2$, 90 mM KCl, and 10 mM NaCl at pH 7.4. Solutions were prepared as follows. Both PNA and RNA were aliquoted from 240 μM stock solutions in water and lyophilized. Buffer (115 μL, 18 μM) was added to the RNA pellet, followed by vortexing and then centrifugation. The solution is then heated to 95 °C for 5 min, then snap-cooled to 4 °C, and left for 5 min. The RNA solution was then combined with the PNA pellet, vortexed, centrifuged, and loaded in a cell of the eight-cell cuvette. Three temperature ramps were done, typically from 10 to 95 °C. The replicates were then used to determine the average and standard deviation in melting temperature (T_m). Detailed results of individual experiments are given in Tables S16−S26 and Figures S30 and S31 and are summarized in Tables S14 and S15.

For melting of RNA hairpins in the absence of PNA, experiments were performed using the same method as above at a concentration of 2.5 μM. Experiments were done in duplicate with absorbance monitored at 260 and 300 nm (Figure S32). No melting was observed at 300 nm (Figure S32B). The results obtained at 260 nm are summarized in Tables S27 and S28.

Circular dichroism (CD) experiments were done on a JASCO J-1100 CD spectrometer at 18 μM concentration in ITC buffer in a cuvette with 2 mm path length. An accumulation of 10 scans from 220 to 360 nm with a scan speed of 20 nm/min and a 1 nm bandwidth was used for all experiments. PNA, RNA, and PNA/RNA complexes were all analyzed to determine changes in CD on complex formation. RNA was dissolved in 230 μL of ITC buffer, heated to 95 °C for 5 min, then snap-cooled to 4 °C, and left for 5 min. RNA was then measured either alone or combined with lyophilized PNA. For PNA, no heat treatment before CD experiments was employed. Representative CD spectra for PNA only, RNA only, and PNA/RNA complexes are shown in Figure S38.

Chemical Probing of PNA−dsRNA Complexes. *RNA Preparation.* Single-stranded DNAs (forward and reverse complement) containing the T7 promoter at the 5′-site, which encoded one- or two-adenosine bulge hairpins (sequences of HRP4 and HRP8), were purchased as Ultramer DNA Oligos from Integrated DNA Technology. The RNAs were transcribed for 16 h at 37 °C using the HiScribe T7 High Yield RNA Synthesis Kit (New England Biolabs). The DNA templates were eliminated from the reaction mixture by RNase free DNase I (Thermo Fisher). After the phenol−chloroform extraction, RNA was precipitated by ethanol and purified using 8% denaturing polyacrylamide gel.

DMS modifications were done following the protocol published by Ikawa and co-workers with the following modification.[26] Briefly, 100 pmol of RNA was dissolved in 11 μL of nuclease-free water in a PCR tube. The solution was incubated at 95 °C for 2 min and immediately placed on ice for at least 2 min. To this solution, 4 μL of 5× reaction buffer (final buffer concentrations: 100 mM HEPES, 2 mM $MgCl_2$, and 100 mM KCl) and 3 μL (300 pmol) of PNA were added. To the negative control tube (no PNA) was added 3 μL of water. The reaction mixtures were allowed to equilibrate at 37 °C for 30 min 2 μL of 10% of DMS in ethanol was added, and the mixture was incubated for 5 min at 37 °C. The reaction was stopped with 25 μL of 1M-mercaptoethanol. After the phenol−chloroform extraction, RNA was precipitated by ethanol and dissolved in 10 μL of water.

SHAPE modifications were done following the protocol published by Weeks and co-workers with the following modification.[27] Briefly, 100 pmol of RNA was dissolved in 11 μL of nuclease-free water in a PCR tube. The solution was incubated at 95 °C for 2 min and immediately placed on ice for at least 2 min. To this solution, 4 μL of

https://doi.org/10.1021/jacs.2c12488
J. Am. Chem. Soc. 2023, 145, 10497−10504

5× reaction buffer (final buffer concentration: 100 mM HEPES, pH 7.5, 2 mM $MgCl_2$, and 100 mM KCl) and 3 μL (300 pmol) of PNA were added. To the negative control tube (no PNA) was added 3 μL of nuclease-free water. The reaction mixtures were allowed to fold at 37 °C for 30 min. To this reaction was added 2 μL of 100 mM 1M7 SHAPE reagent in DMSO and incubated for exactly 75 s at 37 °C. The reaction was terminated with 25 μL of 1M-mercaptoethanol. After phenol−chloroform extraction, RNA was precipitated by ethanol and dissolved in 10 μL of water.

Reverse transcription reactions were conducted according to the manufacturer's recommendations (Invitrogen). Briefly, 1 μL of SHAPE or DMS-modified RNA was mixed with 1 μL of dNTP and 1 μL of IR700-labeled primer complementary to the extended 3′-end of the RNA. To each sequencing reaction, 1 μL of one ddNTP was added. The mixtures were incubated at 65 °C for 5 min and at 37 °C for another 5 min, and the following reagents were added: 2 μL of 10× RT buffer, 2 μL of 25 mM $MgCl_2$, 0.25 μL of 0.1 mM DTT, 0.5 μL of 40 U/μL RNaseOut, and 0.4 μL of 200 U/μL SuperScript III RT. The reaction was incubated for 1 h at 52 °C. The RNA template was removed using 2.0 μL of 2.0 M NaOH. Finally, the cDNA was electrophoresed on a 6% polyacrylamide sequencing gel and analyzed using Typhoon Biomolecular Imager (Figures S34 and S35). Gel analysis and band quantification were carried out using ImageJ.

■ ASSOCIATED CONTENT

Supporting Information

The Supporting Information is available free of charge at https://pubs.acs.org/doi/10.1021/jacs.2c12488.

Detailed results of HPLC purification and LC/MS analysis of PNAs, ITC, UV melting, DMS, and SHAPE probing experiments; native gel shift assays; and CD spectra (PDF)

■ AUTHOR INFORMATION

Corresponding Author

Eriks Rozners − *Department of Chemistry, The State University of New York, Binghamton University, Binghamton, New York 13902, United States;* orcid.org/0000-0001-7649-0040; Phone: (1) 607-777-2441; Email: erozners@binghamton.edu

Authors

Christopher A. Ryan − *Department of Chemistry, The State University of New York, Binghamton University, Binghamton, New York 13902, United States*

Md Motiar Rahman − *Department of Chemistry, The State University of New York, Binghamton University, Binghamton, New York 13902, United States*

Vipin Kumar − *Department of Chemistry, The State University of New York, Binghamton University, Binghamton, New York 13902, United States*

Complete contact information is available at: https://pubs.acs.org/10.1021/jacs.2c12488

Funding

This work was supported by the National Institutes of Health (R35 GM130207 to E.R.).

Notes

The authors declare no competing financial interest.

■ ACKNOWLEDGMENTS

We thank Nikita Brodyagin, Ilze Kumpina, and Brandon R. Tessier for help with the ITC data analysis. This work was supported by the National Institutes of Health (R35 GM130207 to E.R.).

■ REFERENCES

(1) Wang, J. Y.; Pausch, P.; Doudna, J. A. Structural biology of CRISPR−Cas immunity and genome editing enzymes. *Nat. Rev. Microbiol.* **2022**, *20*, 641−656.

(2) Hille, F.; Richter, H.; Wong, S. P.; Bratovič, M.; Ressel, S.; Charpentier, E. The Biology of CRISPR-Cas: Backward and Forward. *Cell* **2018**, *172*, 1239−1259.

(3) Ziv, O.; Price, J.; Shalamova, L.; Kamenova, T.; Goodfellow, I.; Weber, F.; Miska, E. A. The Short- and Long-Range RNA-RNA Interactome of SARS-CoV-2. *Mol. Cell* **2020**, *80*, 1067−1077.

(4) Huston, N. C.; Wan, H.; Strine, M. S.; de Cesaris Araujo Tavares, R.; Wilen, C. B.; Pyle, A. M. Comprehensive in vivo secondary structure of the SARS-CoV-2 genome reveals novel regulatory motifs and mechanisms. *Mol. Cell* **2021**, *81*, 584−598.

(5) Warner, K. D.; Hajdin, C. E.; Weeks, K. M. Principles for targeting RNA with drug-like small molecules. *Nat. Rev. Drug Discovery* **2018**, *17*, 547−558.

(6) Childs-Disney, J. L.; Yang, X.; Gibaut, Q. M. R.; Tong, Y.; Batey, R. T.; Disney, M. D. Targeting RNA structures with small molecules. *Nat. Rev. Drug Discovery* **2022**, *21*, 736−762.

(7) Crooke, S. T.; Baker, B. F.; Crooke, R. M.; Liang, X.-h. Antisense technology: an overview and prospectus. *Nat. Rev. Drug Discovery* **2021**, *20*, 427−453.

(8) Crooke, S. T.; Liang, X.-H.; Baker, B. F.; Crooke, R. M. Antisense technology: A review. *J. Biol. Chem.* **2021**, *296*, 100416.

(9) Zengeya, T.; Gupta, P.; Rozners, E. Triple Helical Recognition of RNA Using 2-Aminopyridine-Modified PNA at Physiologically Relevant Conditions. *Angew. Chem., Int. Ed.* **2012**, *51*, 12593−12596.

(10) Hnedzko, D.; McGee, D. W.; Karamitas, Y. A.; Rozners, E. Sequence-selective recognition of double-stranded RNA and enhanced cellular uptake of cationic nucleobase and backbone-modified peptide nucleic acids. *RNA* **2017**, *23*, 58−69.

(11) Ryan, C. A.; Brodyagin, N.; Lok, J.; Rozners, E. The 2-Aminopyridine Nucleobase Improves Triple-Helical Recognition of RNA and DNA When Used Instead of Pseudoisocytosine in Peptide Nucleic Acids. *Biochemistry* **2021**, *60*, 1919−1925.

(12) Zhou, Y.; Kierzek, E.; Loo, Z. P.; Antonio, M.; Yau, Y. H.; Chuah, Y. W.; Geifman-Shochat, S.; Kierzek, R.; Chen, G. Recognition of RNA duplexes by chemically modified triplex-forming oligonucleotides. *Nucleic Acids Res.* **2013**, *41*, 6664−6673.

(13) Devi, G.; Yuan, Z.; Lu, Y.; Zhao, Y.; Chen, G. Incorporation of thio-pseudoisocytosine into triplex-forming peptide nucleic acids for enhanced recognition of RNA duplexes. *Nucleic Acids Res.* **2014**, *42*, 4008−4018.

(14) Sato, T.; Sakamoto, N.; Nishizawa, S. Kinetic and thermodynamic analysis of triplex formation between peptide nucleic acid and double-stranded RNA. *Org. Biomol. Chem.* **2018**, *16*, 1178−1187.

(15) Tähtinen, V.; Granqvist, L.; Murtola, M.; Strömberg, R.; Virta, P. ^{19}F NMR Spectroscopic Analysis of the Binding Modes in Triple-Helical Peptide Nucleic Acid (PNA)/MicroRNA Complexes. *Chem.—Eur. J.* **2017**, *23*, 7113−7124.

(16) Kim, K. T.; Chang, D.; Winssinger, N. Double-Stranded RNA-Specific Templated Reaction with Triplex Forming PNA. *Helv. Chim. Acta* **2018**, *101*, No. e1700295.

(17) Zhan, X.; Deng, L.; Chen, G. Mechanisms and applications of peptide nucleic acids selectively binding to double-stranded RNA. *Biopolymers* **2022**, *113*, No. e23476.

(18) Brodyagin, N.; Katkevics, M.; Kotikam, V.; Ryan, C. A.; Rozners, E. Chemical approaches to discover the full potential of peptide nucleic acids in biomedical applications. *Beilstein J. Org. Chem.* **2021**, *17*, 1641−1688.

(19) Hermann, T.; Patel, D. J. RNA bulges as architectural and recognition motifs. *Structure* **2000**, *8*, R47−R54.

(20) Buchardt, O.; Egholm, M.; Berg, R. H.; Nielsen, P. E. Peptide nucleic acids and their potential applications in biotechnology. *Trends Biotechnol.* **1993**, *11*, 384−386.
(21) Nielsen, P. E.; Egholm, M.; Berg, R. H.; Buchardt, O. Sequence-selective recognition of DNA by strand displacement with a thymine-substituted polyamide. *Science* **1991**, *254*, 1497−1500.
(22) Aupeix, K.; Le Tinevez, R.; Toulme, J. J. Binding of oligopyrimidines to the RNA hairpin responsible for the ribosome gag-pol frameshift in HIV-1. *FEBS Lett.* **1999**, *449*, 169−174.
(23) Li, M.; Zengeya, T.; Rozners, E. Short Peptide Nucleic Acids Bind Strongly to Homopurine Tract of Double Helical RNA at pH 5.5. *J. Am. Chem. Soc.* **2010**, *132*, 8676−8681.
(24) Brodyagin, N.; Kumpina, I.; Applegate, J.; Katkevics, M.; Rozners, E. Pyridazine Nucleobase in Triplex-Forming PNA Improves Recognition of Cytosine Interruptions of Polypurine Tracts in RNA. *ACS Chem. Biol.* **2021**, *16*, 872−881.
(25) Muse, O.; Zengeya, T.; Mwaura, J.; Hnedzko, D.; McGee, D. W.; Grewer, C. T.; Rozners, E. Sequence Selective Recognition of Double-Stranded RNA at Physiologically Relevant Conditions Using PNA-Peptide Conjugates. *ACS Chem. Biol.* **2013**, *8*, 1683−1686.
(26) Inuzuka, S.; Kakizawa, H.; Nishimura, K.-i.; Naito, T.; Miyazaki, K.; Furuta, H.; Matsumura, S.; Ikawa, Y. Recognition of cyclic-di-GMP by a riboswitch conducts translational repression through masking the ribosome-binding site distant from the aptamer domain. *Genes Cells* **2018**, *23*, 435−447.
(27) Smola, M. J.; Rice, G. M.; Busan, S.; Siegfried, N. A.; Weeks, K. M. Selective 2′-hydroxyl acylation analyzed by primer extension and mutational profiling (SHAPE-MaP) for direct, versatile and accurate RNA structure analysis. *Nat. Protoc.* **2015**, *10*, 1643−1669.
(28) Satpathi, S.; Endoh, T.; Podbevšek, P.; Plavec, J.; Sugimoto, N. Transcriptome screening followed by integrated physicochemical and structural analyses for investigating RNA-mediated berberine activity. *Nucleic Acids Res.* **2021**, *49*, 8449−8461.
(29) Disney, M. D.; Angelbello, A. J. Rational Design of Small Molecules Targeting Oncogenic Noncoding RNAs from Sequence. *Acc. Chem. Res.* **2016**, *49*, 2698−2704.
(30) Childs-Disney, J. L.; Disney, M. D. Approaches to Validate and Manipulate RNA Targets with Small Molecules in Cells. *Annu. Rev. Pharmacol. Toxicol.* **2016**, *56*, 123−140.
(31) Shortridge, M. D.; Varani, G. Structure based approaches for targeting non-coding RNAs with small molecules. *Curr. Opin. Struct. Biol.* **2015**, *30*, 79−88.
(32) Brodyagin, N.; Hnedzko, D.; MacKay, J. A.; Rozners, E. Nucleobase-Modified Triplex-Forming Peptide Nucleic Acids for Sequence-Specific Recognition of Double-Stranded RNA. In *Peptide Nucleic Acids: Methods and Protocols*; Nielsen, P. E., Ed.; Springer US: New York, NY, 2020; pp 157−172.

https://doi.org/10.1021/jacs.2c12488
J. Am. Chem. Soc. 2023, 145, 10497−10504